Supporting Online Material for:

# Helical Structures of ESCRT-III are Disassembled by VPS4

Suman Lata[1], Guy Schoehn[1,2], Ankur Jain[3,†], Ricardo Pires[1], Jacob Piehler[3], Heinrich G. Göttlinger[4] and Winfried Weissenhorn[1,*]

[1] Unit for Virus Host Cell Interaction, UMR 5233 UJF-EMBL-CNRS, 6, rue Jules Horowitz 38042 Grenoble Cedex 9, France

[2] Institut de Biologie Structurale UMR 5075 CEA-CNRS-UJF, 41, rue Jules Horowitz, 38027 Grenoble Cedex 1, France

[3] Institute of Biochemistry, Johann Wolfgang Goethe-University, Max-von-Laue Str. 9, 60438 Frankfurt am Main, Germany

[4] Program in Gene Function and Expression, Program in Molecular Medicine, University of Massachusetts Medical School, Worcester, MA 01605, USA

[*] To whom correspondence should be addressed: weissenhorn@embl.fr

[†]current address: University of Illinois at Urbana-Champaign, Department of Physics, 1110 W. Green Street, Urbana, IL 61801-3080, U.S.A.

The PDF file includes:

**Material and Methods**

**Cloning, protein expression and purification.** CHMP3ΔC containing residues 9 to 183 and CHMP3 containing residues 9-222 were expressed and purified as described (*1*). cDNA fragments derived from human CHMP2A (9-222) and CHMP2AΔC (9-161) were cloned in the expression vector pETM40 using standard PCR methods, which allowed their expression as N-terminal MBP fusion proteins. Similarly, human CHMP4BΔC (1-194) was cloned into expression vector pBADM41 for expression as N-terminal His-MBP fusion protein. cDNA encoding full length VPS4B was cloned into expression vector pProExHTb (Invitrogen). All clones were verified by DNA sequencing.

CHMP3, CHMP3ΔC, CHMP4BΔC and VPS4B were expressed in *E. coli* strain BL21 codon plus™ (Invitrogen) at 37° C for 3 hours. CHMP2A and CHMP2AΔC were expressed in *E. coli* strain C41 at 37° C for 3 and 1 hour respectively. Short induction time for CHMP2AΔC was chosen for its toxic effect on bacterial cell growth.

MBP fusion proteins were applied onto Amylose Resin™ (New England BioLabs) in buffer A (20 mM HEPES, pH 7.6, 300 mM NaCl, 300 mM KCl), bound protein was extensively washed with buffer B (20 mM HEPES, pH 7.6, 1 M KCl or 1 M NaCl) followed by HBS (20 mM HEPES, pH 7.6, 150 mM NaCl). Finally, the proteins were eluted with HBS containing 10 mM Maltose. The samples eluted from the amylose column were spun down by ultracentrifugation using a SW28 rotor at 25,000 rpm (60 min) to remove aggregates. After ultracentrifugation monomeric proteins were isolated by subjecting the supernatant to size exclusion chromatography (SEC) in HBS. The MBP moiety was not removed from CHMP2AΔC and CHMP4BΔC, since removal resulted in protein aggregation.

His-tagged proteins were purified by immobilized metal ion chromatography (IMAC) by using the His-trap™ chelating column (GE Healthcare). Proteins were loaded on the column in buffer A followed by extensive washing with buffer B and HBS. The proteins were eluted

with a linear gradient of imidazole in HBS. His-tags were cleaved off by using TEV protease, and cleaved protein was separated from the uncleaved material by another round of IMAC. The flow through was then subjected to SEC in HBS. For VPS4B, DTT was added to a final concentration of 100 μM. All proteins were stored at 4°C and were used for polymer formation within the first 4 to 5 days. No significant difference in the aggregation behavior over this period was observed for any of the proteins used in this study.

**Large unilamellar vesicle (LUV) preparation.** Synthetic 1-Stearoyl-2-Oleoyl-*sn*-Glycero-3-Phosphocholine (SOPC) and 1,2-Dioleoyl-*sn*-Glycero-3-Phosphoserine (DOPS) were bought from Avanti Polar Lipids. Different lipid species were homogeneously mixed in chloroform in appropriate proportions for any desired lipid composition. Dried thin lipid films in a round bottom flask were obtained by evaporating organic solvents. Lipid films were hydrated with HBS to a final concentration of 2 mg/ml. The translucent solution was warmed to 37° C and then extruded 21 times through a 400 nm polycarbonate membrane (Avanti Polar Lipids) followed by centrifugation to obtain large uni-lamellar vesicles (SUVs) in the supernatant.

**ESCRT-III polymer preparation.** ESCRT-III proteins and lipids were mixed in the following concentrations:

Table 1

| | CHMP2AΔC [μM] | CHMP3ΔC [μM] |
|---|---|---|
| Figure1A | 15 | 40 |
| Figure1B | 15 | 30 |

Table 2

| | CHMP2AΔC [μM] | CHMP3ΔC [μM] |
|---|---|---|
| Figure2A | 15 | 30 |
| Figure2B | 15 | 30 |

Table 3

| | CHMP2AΔC [μM] | CHMP3 [μM] | VPS4B [μM] | ATP.Mg [μM] |
|---|---|---|---|---|
| Figure3A | 10 | 15 | 0 | 0 |
| Figure3B | 10 | 0 | 0 | 0 |
| Figure3C | 0 | 30 | 0 | 0 |
| Figure3D | 0 | 0 | 10 | 0 |
| Figure3E | 7 | 7 | 7 | 0 |
| Figure3F | 7 | 7 | 7 | 200 |
| Figure3G | 10 | 15 | 40 | 0 |
| Figure3J | 10 | 15 | 40 | 200 |

Table 4

| | CHMP2AΔC [μM] | CHMP3ΔC [μM] | SOPC [mg/ml] | 20%DOPS:SOPC [mg/ml] |
|---|---|---|---|---|
| Figure4C | 15 | 30 | 0 | 0 |
| Figure4D | 15 | 30 | 0 | 0 |
| Figure4E | 10 | 15 | 0.5 | 0 |
| Figure4F, (right panel), G, H | 10 | 15 | 0 | 0.5 |
| Figure4F, (left panel), G, H | 10 | 15 | 0 | 1.5 |

Table 5

| | CHMP2AΔC [μM] |
|---|---|
| FigureS1C | 40 |

Table 6

| | CHMP2AΔC [μM] | CHMP3ΔC [μM] | CHMP3 [μM] | 20%DOPS:SOPC [mg/ml] |
|---|---|---|---|---|
| FigureS9A | 0 | 20 | | 0.5 |
| FigureS9B | 10 | 0 | 0 | 0.5 |
| FigureS9C | 10 | 20 | | 0.5 |
| FigureS9D | 10 | 0 | 20 | 0.5 |

**Sucrose density gradient ultracentrifugation.** Sucrose gradients were prepared manually in ultracentrifuge tubes with 40 % (w/v) sucrose in HBS at the bottom followed by equal volume fractions of 30, 20, 10 and 5 % (w/v) sucrose, all in HBS. Protein or protein-complexes in HBS were then applied on top, followed by ultracentrifugation in a swing bucket rotor SW55Ti (Beckman Coulter) at 45-50k rpm for 6-12 h at 10° C. Soluble monomeric proteins

stay in the upper fractions and high molecular weight oligomers migrate to the bottom of the gradient.

Sucrose gradients for floatation experiments were prepared as follows: Proteins and LUVs were mixed with an equal volume of 80 % (w/v) sucrose in HBS resulting in a final sucrose concentration of 40 % (w/v), which was applied at the bottom of the ultracentrifuge tubes followed by equal volume layers of 30, 20, 10, 5, and 0 % (w/v) sucrose in HBS. The tubes were then subjected to ultracentrifugation in a SW55Ti swing bucket rotor at 45-50k rpm for 4 h at 15° C. Due to a large difference in density in the interior and the exterior of the lipid vesicles, LUVs float to the upper sucrose fractions (0 % (w/v)) and proteins or protein polymers stay at the bottom, interactions between protein polymers and LUVs leads to a re-distribution of LUVs and proteins across the gradient. After ultracentrifugation gradients were fractionated and analyzed by SDS PAGE, protein and lipid bands were visualized by Coomassie brilliant blue staining.

**Electron microscopy.** Samples were applied to the clean side of carbon on mica (carbon/mica interface) and negatively stained with 2% sodium silicotungstate (pH 7.0). A grid was placed on top of the carbon film covered by the sample, which was subsequently air-dried. Micrographs were taken with a JEOL 1200 EX II microscope at 100 kV and a calibrated magnification of 39,750 times (using the Tobacco Mosaic Virus particle). Selected negatives were then digitized on an EPSON scanner with a pixel size of 10.6 μm 2400 dpi (2.65 Å at the sample scale). Vitrified samples were prepared according to the method of Dubochet et al., (*2*). 3 μl of sample (CHMP2AΔC-CHMP3ΔC tubes; MBP attached to CHMP2AΔC) at about 1 mg/ml were applied to R2/2 quantifoil grids (Quantifoil Micro Tools GmbH, Germany)). The excess liquid was blotted with filter paper for 1–2 s and rapidly plunged into liquid ethane at −175 °C. Specimens were observed with a GATAN cryo-transfer stage on a Philips CM200 microscope at 200 kV. Images were recorded on Kodak SO 163 film under low-dose conditions (<10 $e^{-}/Å^{2}$) at a nominal magnification of 38,000× (39,500 according to TMV calibration) with defocus values between 1.2 μm and 2.5 μm. Micrographs were digitized on a

Zeiss Photoscan TD scanner with a pixel size of 7 μm (corresponding to a pixel size of 1.77 Å at the specimen).

**Iterative real space helical reconstruction of the CHMP2AΔC-CHMP3ΔC co-polymer.** 4400 sections of tubes were selected and interactively boxed into boxes with 480×480 pixels. The resulting images were binned into boxes with 240×240 pixels using a pixel size of 3.54 Å. Particles were selected manually with an overlap of ~2/3 of a box. These images were used to determine the defocus using SUMPS and CTFZEROS (*3*). The data was then corrected for the contrast transfer function (CTF) corresponding to the defocus value of the image by flipping the phases. The resolution limit in the images was considered to be 15 Å, as this was the distance of the last visible zero of the CTF. The iterative helical real space reconstruction method (IHRSR) as implemented in SPIDER was applied to solve the structure of the CHMP2AΔC/CHMP3ΔC polymers (*4*) (*5*). As a starting model for the image alignment and search for image classes a continuous smooth helix with a pitch of 32 Å was used. The pitch has been measured using the power spectrum of different tubes. After 120 cycles of the IHRSR procedure using a 2-degree step for reprojecting the map perpendicular to its axis, the starting model converges to a helix with a pitch of 32 Å and 16.57 subunits per turn. Only the 2500 images, which showed the best correlation coefficient with the re-projections were retained and employed for calculating the final reconstruction. For all the IHRSR steps only the density derived form the CHMP proteins was taken into account; the extra density, which most likely derives from MBP attached to CHMP2AΔC via a flexible linker was excluded. Thus the diameters of the reconstruction and projections have been limited to the inner helix (ie diameter shorter than 260 Å).

The resolution of the reconstruction has been estimated to be 30 Å by Fourier shell correlation. Although the number of images used in the reconstruction should generally produce models with a higher resolution as shown previously for helical reconstructions (*6*),

the failure to obtain a higher resolution may be due to two reasons. First, the employment of MBP-tagged CHMP2AΔC particles may have diminished or blurred the information by the random orientations of MBP. This thus affected the alignment of the original EM images to the re-projection of the CHMP2AΔC-CHMP3ΔC tubes. Secondly, the irregular diameter (the number of repeating units per turn) along the tubular structures limited the amount of particles, which could be analyzed. Furthermore helices with the same apparent diameter may have distinct helical symmetries, preventing reciprocal space averaging (*7*). Removal of MBP by TEV protease cleavage is not an option to improve particle selection and alignment since it leads to aggregation of the tubular structures.

The radial density profiles have been calculated using the program SPIDER (*5*). Top view images have been centered by cross correlation with a centered circle, and their rotational averages calculated (*5*). The radial densities have then been plotted using Kaleidagraph and superimposed with the original images.

The EM map has been deposited in the EM database associated with the Macromolecular Structure Database at the European Bioinformatics Institute under accession number EMD-1536.

**Molecular fit of a CHMP2A-CHMP3 model into the EM map.** Since CHMP3 and CHMP3ΔC did not dimerize/polymerize on their own, the helical co-polymerization of CHMP2A and CHMP3 requires at least two hetero-dimer interfaces. The CHMP3 crystal structure revealed two alternative dimers based on crystallographic packing. Both dimerization interfaces have been shown to be functional since they are required for HIV-1 budding (*1*). Because most of the interactions would be conserved in a CHMP2A-CHMP3 heterodimer based on the CHMP3 crystal structure (*1*) and the sequence identity/alignment between CHMP2A and CHMP 3 (23.9 %), a CHMP2A-CHMP3 heterodimer model (fig.S2A and B) was constructed based on the CHMP3 crystallographic homodimer. Helix 5 was omitted in the

model due to its flexible linkage to the core of CHMP3. The CHMP2A-CHMP3 dimer model was manually placed into the repeating unit of the EM map exposing the membrane binding surface to the outside and the C-terminal end comprising the VPS4B binding site towards the interior of the tube. The repeating unit is in accordance with the observed polymer growth which terminates perpendicularly flat to the longitudinal axis of the cylinder and thus produces generally straight ends of polymers. Although the current map with its limited resolution does not allow to unambiguously placing the dimer into the repeating unit, the dimer position shown in fig. S2 produced a helical polymer model with a cross correlation coefficient of 93.1 and an $R_{factor}$ of 43% (after rigid body refinement), when the symmetry operators were applied by using the program UROX (http://mem.ibs.fr/UROX/index.html).

.

**CHMP4BΔC and CHMP2AΔC-CHMP3ΔC polymer formation.** In order to determine whether or not CHMP4BΔC could become an integral part of the tubular structures formed by CHMP2AΔC and CHMP3ΔC, we incorporated CHMP4BΔC in the co-polymerization experiment. CHMP2AΔC (12μM), CHMP3ΔC (30μM, histidine tag cleaved off by the TEV protease) and CHMP4BΔC (12μM) were mixed together and subjected to sucrose density gradient ultracentrifugation. The bottom fraction showed all the three proteins on an SDS-PAGE (fig. S3A) and negative staining EM revealed tubular structures similar to those formed by CHMP2AΔC-CHMP3ΔC alone. In order to probe whether or not these structures contained CHMP4BΔC, we prepared 10 nm sized gold particles coated with tris-NTA. Briefly, an access of tris-NTA conjugated with biotin ($^{BT}$tris-NTA, fig. S3B, C and D) was mixed with gold particles coated with streptavidin, the access of $^{BT}$tris-NTA was removed by SEC, and thereby generating gold particles capable of recognizing histidine tagged proteins (in this case CHMP4BΔC). Gold labeled $^{BT}$tris-NTA was incubated with complexes formed by

CHMP2AΔC, CHMP3ΔC and CHMP4BΔC, which were purified over a sucrose gradient prior to negative staining EM.

**Polymer disassembly**. CHMP2AΔC/CHMP3 co-polymer was separated from the monomeric proteins by density gradient ultracentrifugation as described above. After 5 fold dilution of the bottom fraction the sample was centrifuged again. The pellet was extensively washed and re-suspended in HBS. For amine specific labeling of the co-polymer, 5-iodoacetamidofluorescein was freshly dissolved in HBS and reaction was carried out at room temperature for 1 hour at a final protein concentration of 2 mg/ml and 100 μM of the fluorophore. The reaction mixture was centrifuged and the pellet was extensively washed in order to remove free fluorophore followed by resuspension in HBS. Finally, the labeled co-polymer was re-suspended in HBS. The protein concentration was estimated to be ~1 mg/ml on SDS-PAGE by using the Precision Plus Protein$^{TM}$ standards from Biorad. Fluorescein concentration was determined to be 16 μM by measuring absorption at 490 nm. Taken together these numbers indicated a labeling efficiency of ~1.3 fluorophores per CHMP2AΔC/CHMP3 dimer. For monitoring the disassembly of the polymer (Figure S3) the labeled CHMP2AΔC-CHMP3 substrate was transferred at a final protein concentration of 0.1 mg/ml into the cuvette containing either (i) HBS, (ii) VPS4B (10μM), (iii) VPS4B (10 μM) and AMP-PNP.$Mg^{2+}$ (100 μM), (iv) VPS4B (5 μM) and ATP.$Mg^{2+}$ (50 μM), or (v) VPS4B (10 μM) and ATP.$Mg^{2+}$ (100 μM). Emission intensity was measured at 520 nm as a function of time by exciting fluorescein at 490 nm using a PTI-QM4 fluorospectrometer.

**Binding of the ESCRT-III on solid supported planar lipid bilayers.** Label-free binding assays by reflectometric interference spectroscopy (RIfS) were carried out as previously described using a home-built set-up with a data acquisition rate of 1 Hz. For bilayer assembly,

cleaning of the transducer surface and small unilamellar vesicles (SUVs) preparation was done as described before (*10*). While SUVs composed of neutral lipids, such as SOPC, bind and fuse with great ease on silica surface (*8*), due to electrostatic repulsion, negatively charged SUVs are not readily deposited. In order to minimize the electrostatic repulsion between negatively charged 20% DOPS:SOPC SUVs and the silica surface, NaCl concentration was adjusted to 1 M before injection. A maximum mass deposition of ~5.5 ng/mm$^2$ was observed which is typical for bilayer formation (fig. S6B). Freshly assembled silica supported bilayers were cleaned for loosely bound lipids, if any, with 1M NaCl in HBS, no significant mass removal was observed, followed by an injection of Maltose Binding Protein (30 μM) which resulted in no significant mass deposition, thus demonstrating the integrity of a perfectly formed lipid bilayer (fig. S6B). For measuring protein-bilayer interaction, proteins or protein-complexes were injected at a concentration of 4 μM on SOPC or 20% DOPS:SOPC bilayers for 50 s. Dissociation was typically measured for 250 s and dissociation rate constants ($k_d$) were determined by fitting a mono-exponential function to the dissociation phase.

**Exchange dynamics of the ESCRT-III on solid supported planar lipid bilayers.** The dynamics within the membrane-bound CHMP2AΔC-CHMP3ΔC complex was probed using total internal reflection fluorescence spectroscopy (TIRFS) in combination with reflectometric interference detection and carried out with a data acquisition rate of 1 Hz (*8*)(*9*). His-tagged CHMP3AΔC-H6 and CHMP2AΔC were deposited together on DOPS:SOPC bilayers, at concentrations of 2 μM each for 100 s which led to a mass deposition of 2.36 ng/mm$^2$ (fig. S8A), followed by in situ fluorescence labeling with $^{OG488}$tris-NTA (Fig S8A). $^{OG488}$tris-NTA carries a fluorophore Oregon Green 488 (OG488) and three nitrilotriacetic acid (NTA) moieties (fig S8B) which bind hexa-histidine tags with sub-nanomolar affinity (*11*)(*12*). In order to monitor the exchange dynamics of CHMP3ΔC, another injection of non-labeled

CHMP3ΔC at a concentration of 50 μM was performed which led to mass deposition of 0.97 ng/mm$^2$. No appreciable change in fluorescence intensity either during or after the injection implied that, once assembled on a bilayer, the CHMP2AΔC-CHPM3ΔC co-polymer did not exchange with the soluble or with the membrane bound CHMP3ΔC (fig S8A). We followed the CHMP3ΔC injection with an injection of CHMP2AΔC-CHMP3ΔC (2 μM each) which led to a mass deposition of 1.62 ng/mm$^2$. Once again no appreciable change in fluorescence intensity either during or after the injection (fig. S8A) suggested little, if any, dynamics within the CHMP2AΔC-CHMP3ΔC co-polymer.

**Illustrations.** Molecular representations (fig. S2) were produced with PyMOL (http://pymol.sourceforge.net).

## Supplementary figures

**Figure S1: Schematic overview of CHMP constructs and oligomerisation of CHMP2AΔC.**

(A) Schematic drawing of CHMP2A and CHMP3 constructs used. Helical secondary structure elements are based on crystal structures (*1, 14, 15*), N-terminal basic core, blue; C-terminal acidic region, red. Based on the level of sequence similarity between CHMP3 and CHMP2A, the same secondary structure content has been assigned for CHMP2A.

(B) Superdex 200 gel filtration analysis of CHMP2AΔC. The exclusion volume and the elution volume for MBP are indicated by dotted lines.

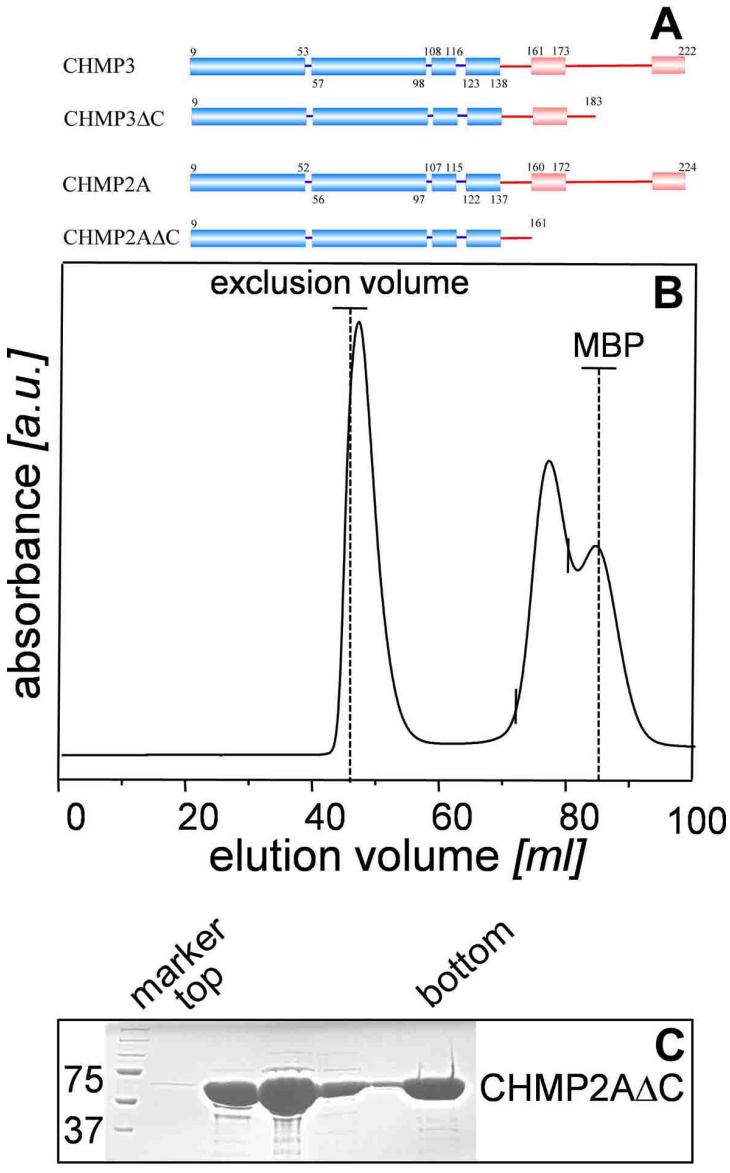

(C) Sucrose gradient analysis of CHMP2AΔC. The proteins were applied on top of the gradient. After ultracentrifugation the gradients were fractionated and analyzed by SDS-PAGE. Part of the protein floated in the upper fractions representing the soluble forms, while protein in the bottom fractions indicated the formation of high molecular weight polymers.

**Figure S2. Molecular fit of the CHMP2A-CHMP3 model into the EM map**

(A) Ribbon representation of a CHMP2A-CHMP3 heterodimer model based on the crystallographic CHMP3 dimer 1 (*1*).

(B) The anti-parallel dimerization mode present in dimer 1 generates a slightly curved surface as shown in the side view. CHMP3 dimerization with CHMP2A may thus use a similar structural principle to generate a curved membrane interaction surface as described for BAR and F-BAR domains (*7, 16-19*).

(C) Ribbon representation of the crystallographic CHMP3 dimer 2 (*1*) that shows interactions via the tips of the helical hairpins.

(D) Molecular fit of the CHMP2A-CHMP3 heterodimer model 1 into the proposed repeating unit of the EM map. Three consecutive models are shown related by the helical symmetry of the EM model.

(E) The molecular fit of model 1 (placed into the repeating unit in D) as viewed down the helical axis after application of the helical symmetry operators. The 45 Å width of the EM map accommodates the flat helical assembly of CHMP2A-CHMP3 complexes.

Although the EM map shows too little features to unambiguously place the proposed heterodimer model, polymerization of the assigned repeating unit (CHMP2A-CHMP3 heterodimer) would encompass lateral CHMP protein interactions overlapping with those observed in the crystallographic CHMP3 dimer 2 (C).

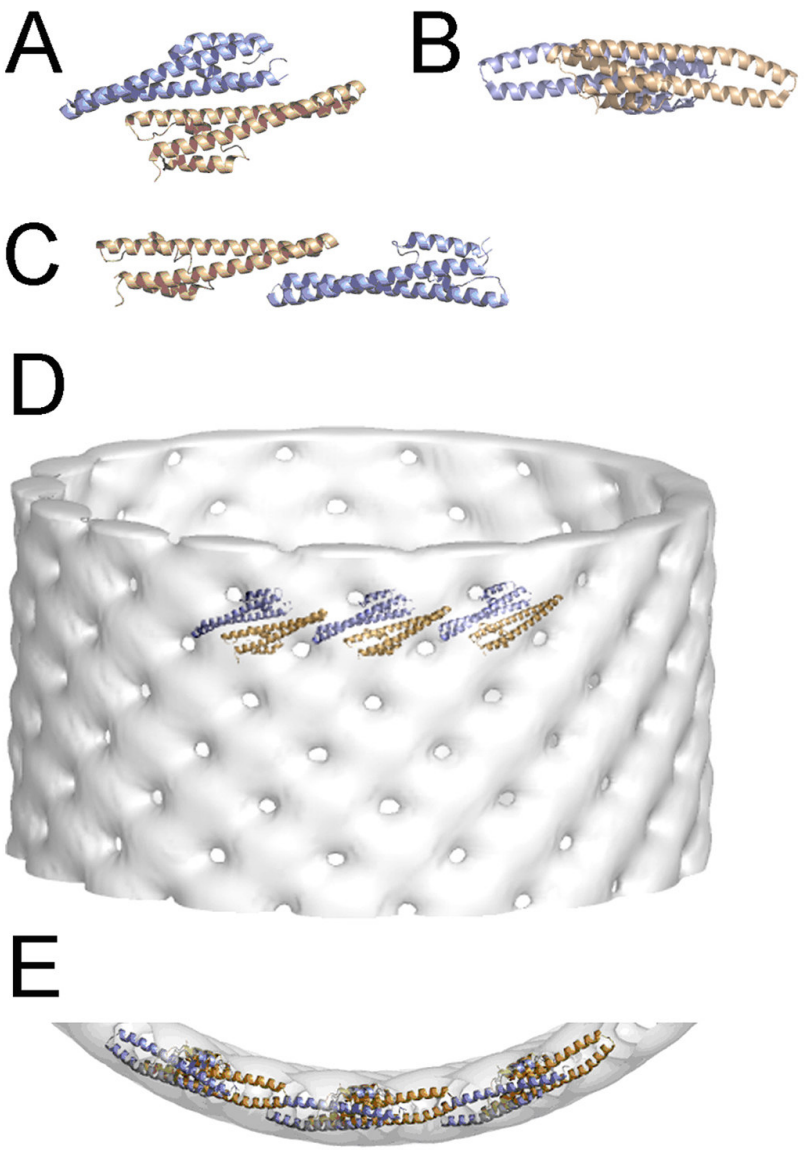


**Figure S3. CHMP4BΔC does not incorporate into CHMP2AΔC-CHMP3ΔC tubes.**

(A) CHMP2AΔC (no HIS-tag) (12μM), CHMP3ΔC (His-tag removed; 30μM) and CHMP4BΔC (attached to His-tagged MBP; 12μM) were mixed and high molecular weight complexes were purified over a sucrose gradient. The bottom fraction (next to the marker lane) contained all three proteins as determined by SDS-PAGE.

(B) Chemical structure of Biotin conjugated tris-NTA loaded with Ni(II) ions ($^{BT}$-trisNTA),

(C) Biotin and tris-NTA recognize streptavidin and HIS-tagged proteins respectively,

(D) Gold particles exposing streptavidin on their surface bind $^{BT}$-tris-NTA conjugates, which was used for gold labeling of His-tagged CHMP4BΔC.

(E) Negative staining EM showed filament structures of CHMP4BΔC labeled with gold particles and (F) tubular CHMP2AΔC-CHMP3ΔC polymers and gold labeled particles in the background; the right panel shows a CHMP4BΔC filament that may be attached to the tube.

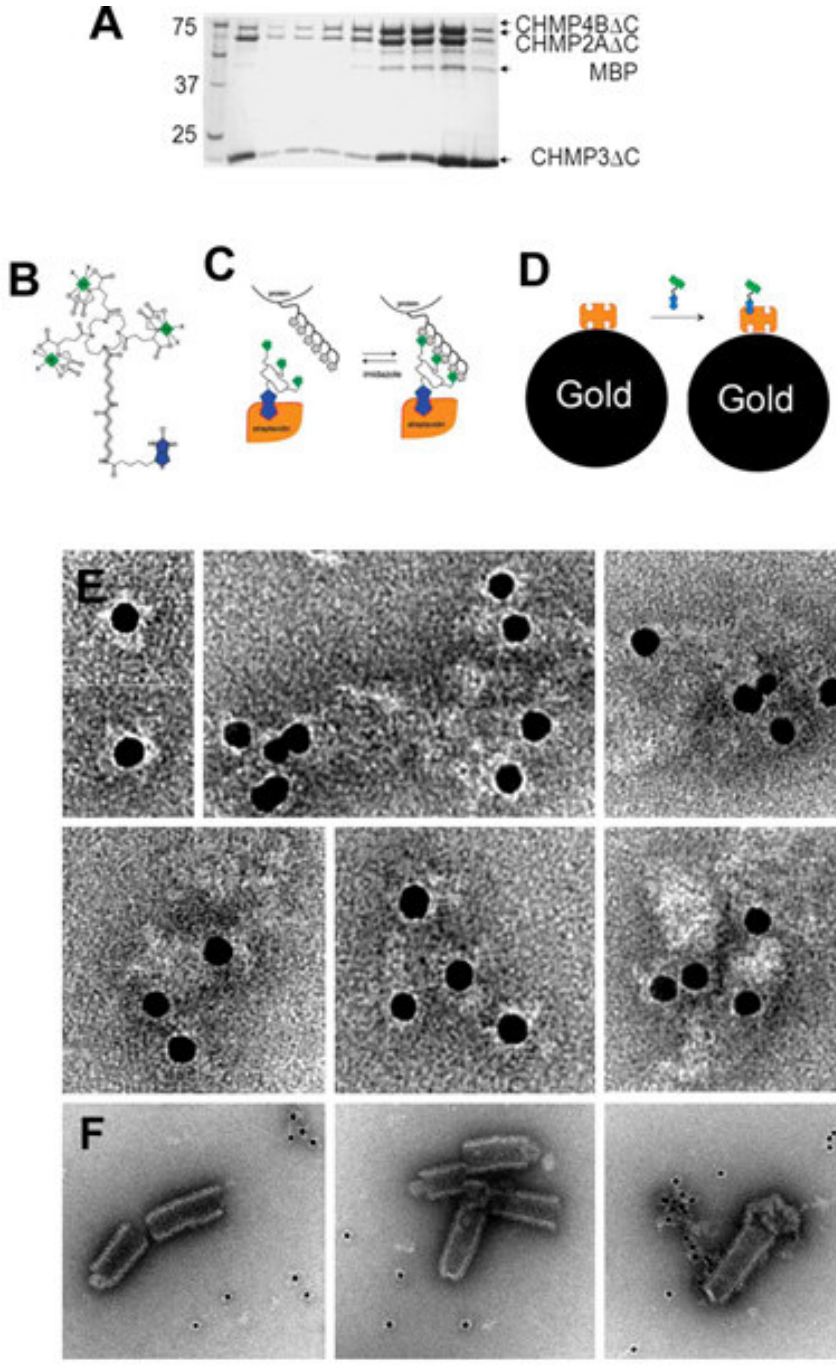

**Figure S4. Cryo-EM analysis of CHMP2AΔC-CHMP3 tubes in the absence and presence of VPS4B.**

(A) Cross sections of tubular helical structures of CHMP2AΔC-CHMP3 alone and (B) with VPS4B inside.

(C) Radial density profiles of CHMP2AΔC-CHMP3 tubes alone and (D) CHMP2AΔC-CHMP3 tubes in the presence of VPS4B.

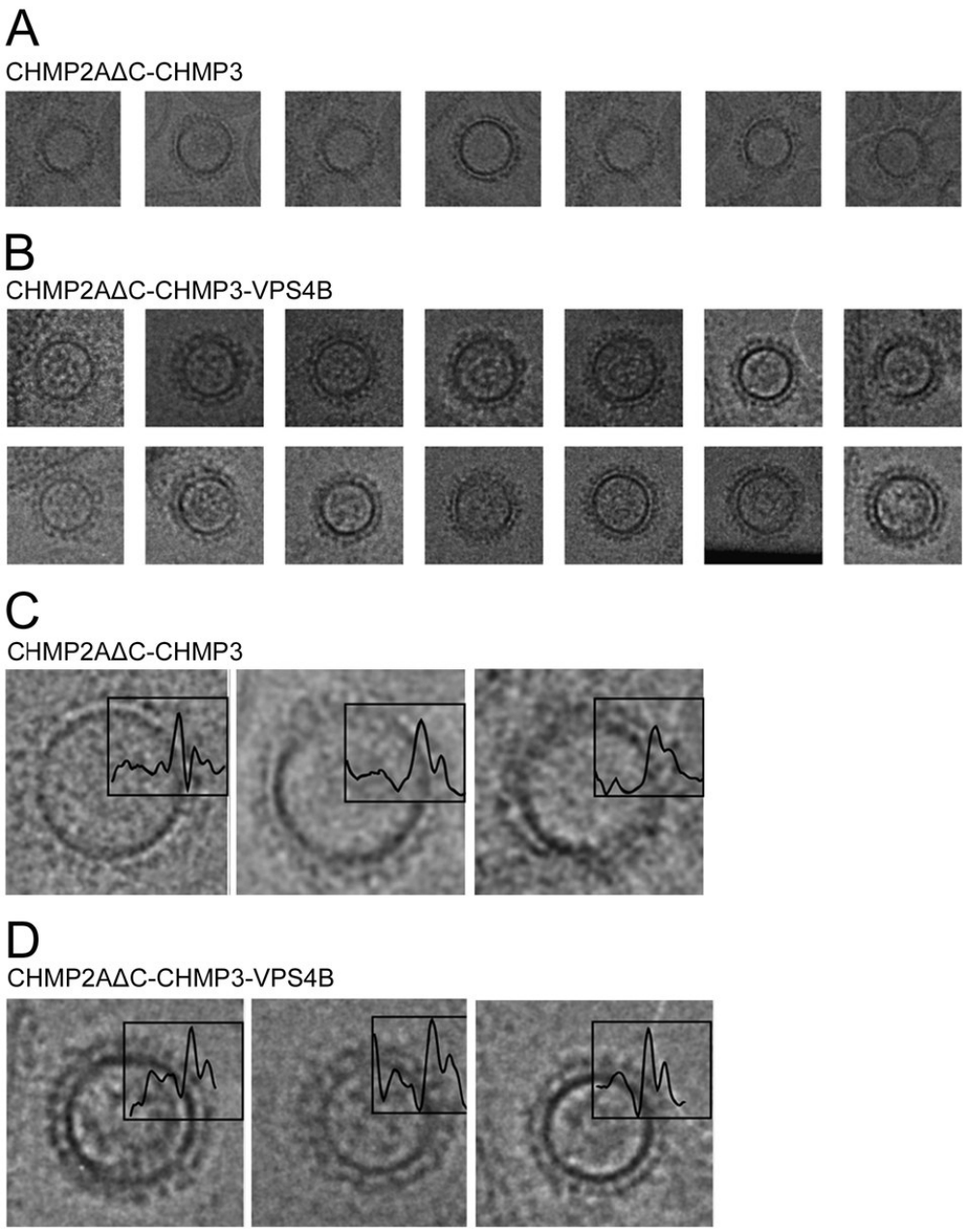

**Figure S5. Fluorescence dequenching**

Schematic representation of fluorescein labeled CHMP2ΔC/CHMP3 copolymer: Fluorescence may quench by energy transfer among the neighboring fluorescein molecules. Upon disassembly the increased distance between the fluorophores leads to fluorescence recovery.

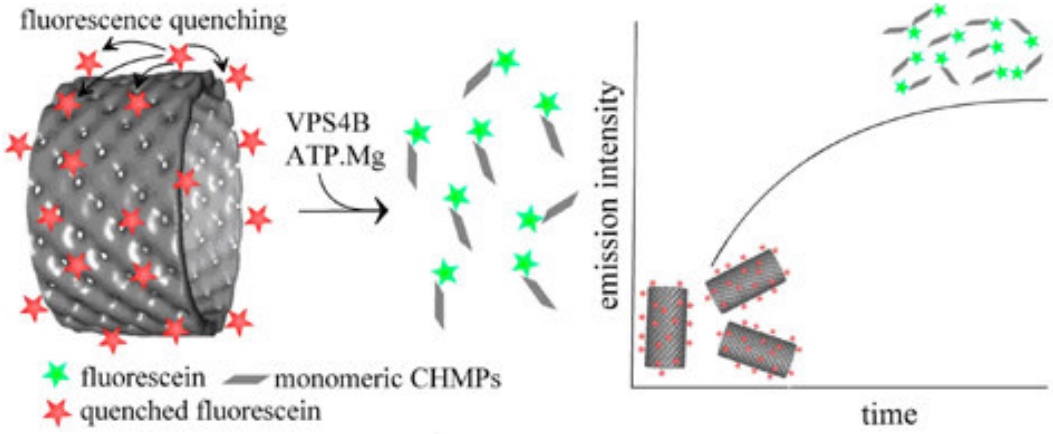


**Figure S6. Bilayer assembly on silica support measured by RIfS**

(A) Schematic representation of the injection scheme and (B) the RIfS binding curves. (1) Fusion of 20% DOPS:SOPC SUVs on the silica surface, (2) washing with 1M NaCl in HBS, (3) injection of MBP and, (4) washing with 1M NaCl in HBS.

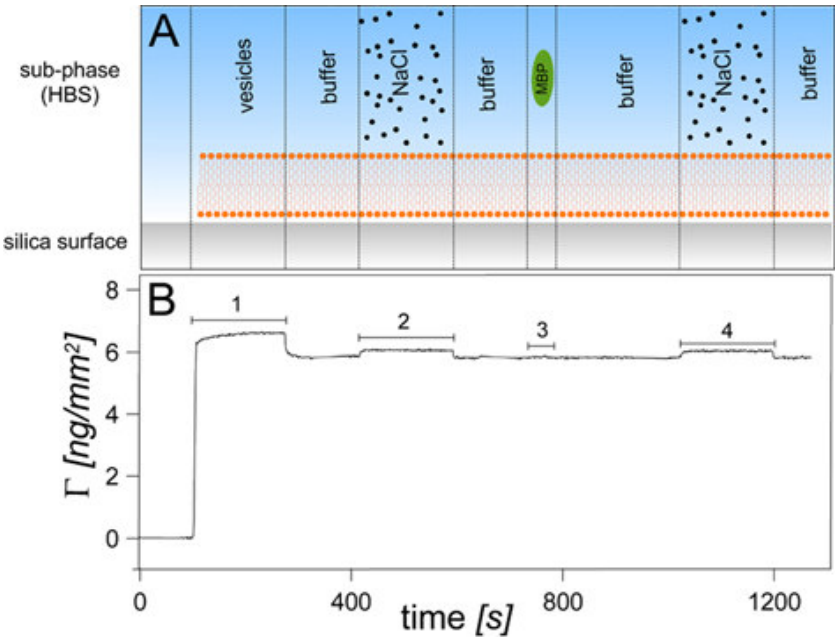

**Figure S7. Dissociation kinetics of CHMP2AΔC, CHMP3ΔC and CHMP2AΔC-CHMP3ΔC complexes from DOPS:SOPC silica supported lipid bilayers.** The dissociation phases and the fits are shown for a mono-exponential function. CHMP3ΔC (magenta), CHMP2AΔC (green), (iii) CHMP2AΔC-CHMP3ΔC complex (blue) and, (iv) CHMP2AΔC-CHMP3ΔC complex upon injection of 1 M NaCl in HBS (blue).

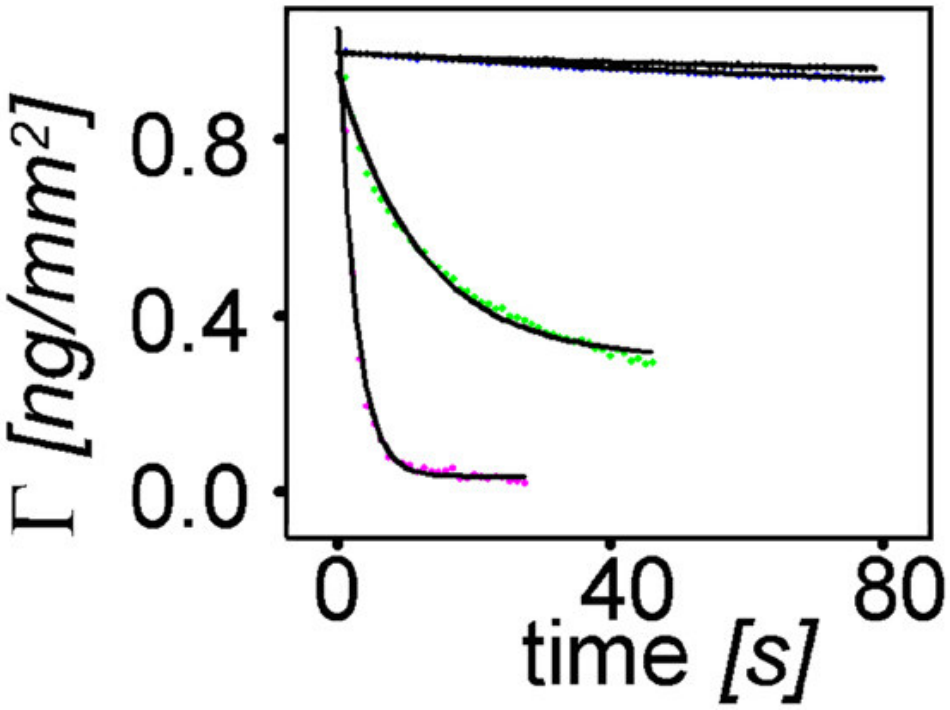


**Figure S8. Exchange dynamics of the CHMP2AΔC-CHMP3ΔC complex.** The dynamics of the CHMP2AΔC-CHMP3ΔC complex formation on a silica supported DOPS:SOPC bilayer was further probed using total internal reflection fluorescence spectroscopy (TIRFS) in combination with reflectometric interference (RIf). (A) His-tagged CHMP3ΔC and CHMP2AΔC were assembled on a DOPS:SOPC bilayer ($\Gamma$= 2.36 ng/mm$^2$) (step 1) followed by *in situ* fluorescence labeling of CHMP3ΔC (step 2) with $^{OG488}$tris-NTA. Additional injection of non-labeled CHMP3ΔC (50μM) led to a $\Gamma_{eq}$ of 0.97 ng/mm$^2$ (step 3); however, no substantial change in fluorescence intensity could be observed either during or after the

injection implying that once assembled on a bilayer, the CHMP3ΔC-CHMP2AΔC complex neither exchanged with soluble CHMP3ΔC nor with membrane bound CHMP3ΔC. Injection of CHMP3ΔC/CHMP2AΔC (2μM) (step 4) led to additional deposition ($\Gamma_{eq}$ = 1.62 ng/mm$^2$) but again no change in fluorescence intensity indicated little, if any, dynamics in the complex. (B) Chemical structure of $^{OG488}$tris NTA.

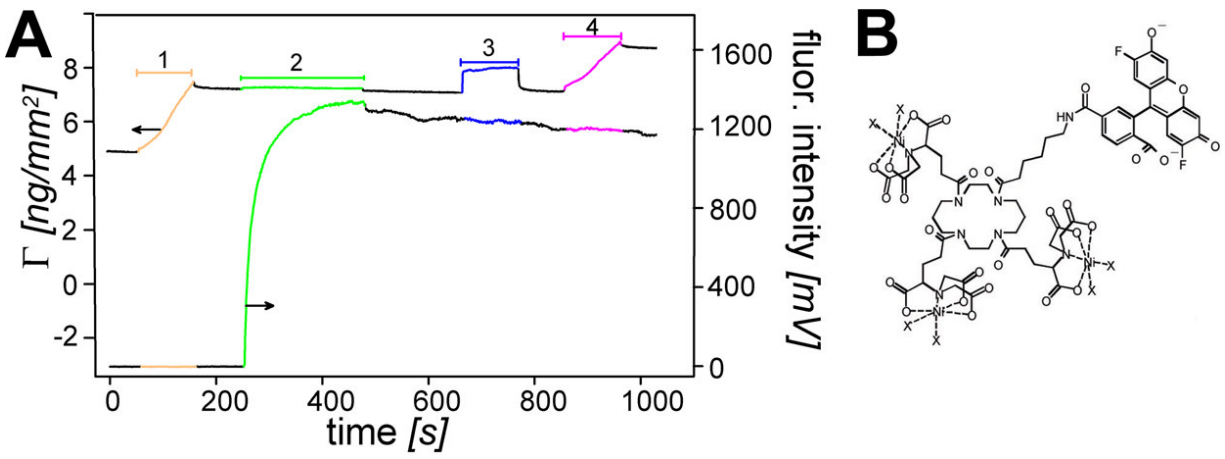


**Figure S9. Effect of CHMPΔC proteins on SOPC: DOPS LUVs.** Sucrose gradient centrifugation of CHMP proteins in the presence of DOPS:SOPC LUVs. The reaction mixture was applied at the bottom of the centrifuge tube. After ultracentrifugation, the fractions were analyzed by SDS-PAGE. Proteins and lipids were visualized by Coomassie brilliant blue staining: (A) CHMP3ΔC; (B) CHMP2AΔC; (C) preassembled CHMP2AΔC-CHMP3ΔC tubes and (D) Preassembled CHMP2AΔC-CHMP3 tubes (MBP was removed from CHMP2AΔC by TEV protease cleavage).

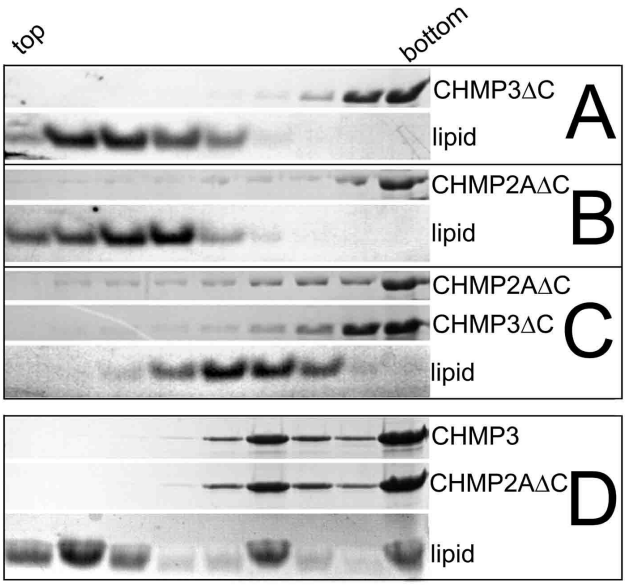


**Figure S10. Model for ESCRT-III helical polymer function.**

(A, B, upper panels) Short helical tubular structures assemble on the inside of a newly formed bud with their C-termini exposed towards the 45 nm wide cavity. CHMP binding proteins interacting with the C-terminal regions of CHMPs such as AMSH (*20*) or Alix (*21*) might determine which CHMP proteins stay within the polymer and which are accessible to be removed by VPS4.

(A, middle and lower panels) Selective removal of CHMP proteins may lead to constriction and may involve the formation of the CHMP2A ring-like structure which could be directly involved in final budding steps; alternatively, it might be the end product after membrane fission.

(B, middle and lower panels) The cone-shaped closed tubular structures formed by CHMP2AΔC and CHMP3ΔC in the presence of DOPS:SOPC LUVs might represent an assembly that could support an intermediate stalk or hemifusion state (*22*), since a bilayer could wrap around the curved structure and thus stabilize this intermediate state. Such a structure could prevent leakage during separation of two bilayers because the CHMP protein polymer could seal the opening.

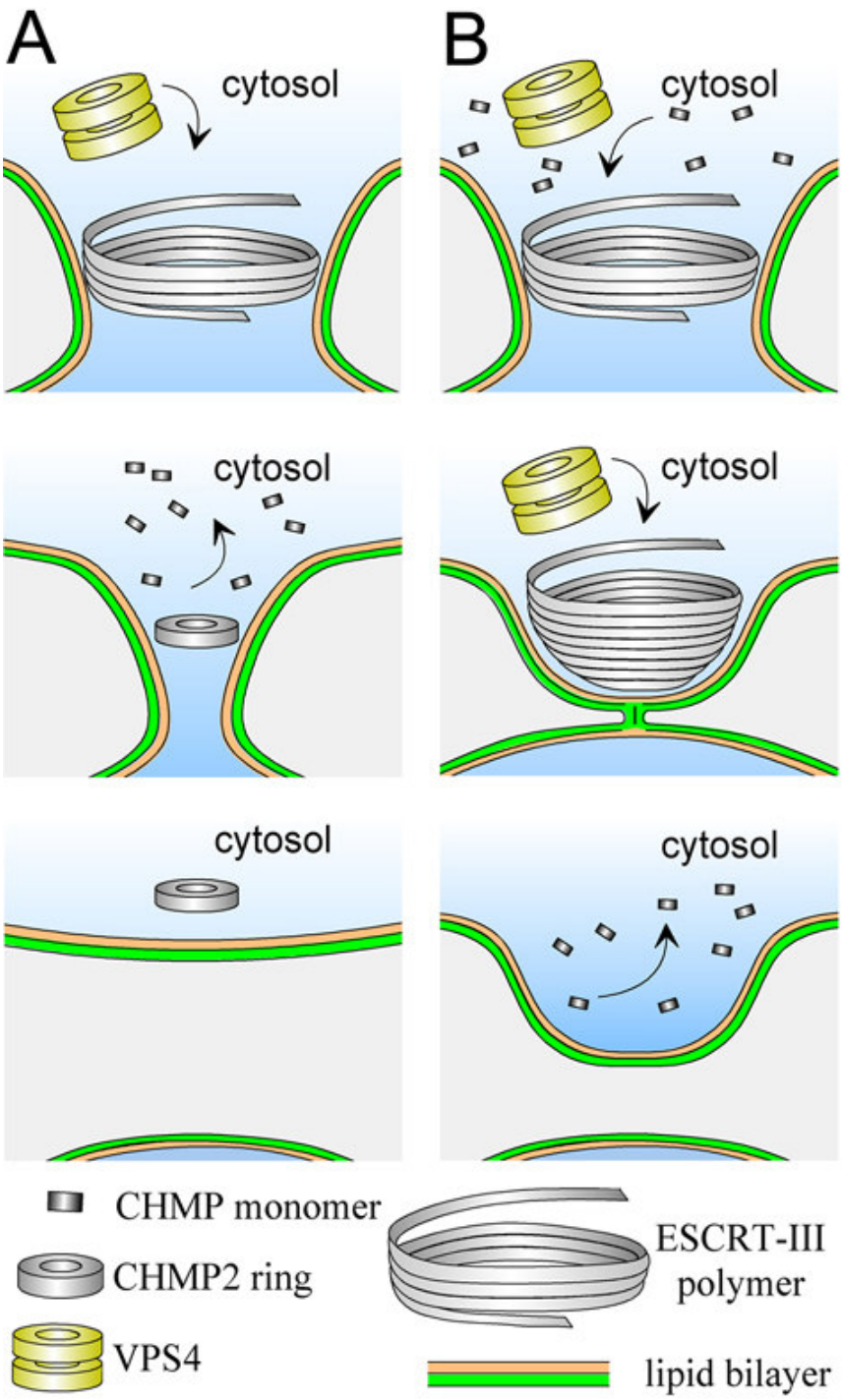
A
B
cytosol
cytosol
cytosol
cytosol
cytosol
cytosol
CHMP monomer
CHMP2 ring
VPS4
ESCRT-III
polymer
lipid bilayer

**References**


1. T. Muziol, E. Pineda-Molina, R. B. Ravelli, A. Zamborlini, Y. Usami, H. Gottlinger, W. Weissenhorn, *Dev Cell* **10**, 821-30 (2006).
2. J. Dubochet, M. Adrian, J. J. Chang, J. C. Homo, J. Lepault, M. A.W., P. Schultz, *Q Rev Biophys.* **21**, 129-228 (1988).
3. J. F. Conway, A. C. Steven, *J Struct Biol* **128**, 106-18 (1999).
4. E. H. Egelman, *Ultramicroscopy* **85**, 225-34 (Dec, 2000).
5. J. Frank, M. Radermacher, P. Penczek, J. Zhu, Y. Li, M. Ladjadj, A. Leith, *J Struct Biol* **116**, 190-9 (1996).
6. G. Schoehn, M. Mavrakis, A. Albertini, R. Wade, A. Hoenger, R. W. Ruigrok, *J Mol Biol* **339**, 301-12 (2004).
7. A. Frost, R. Perera, A. Roux, K. Spasov, O. Destaing, E. H. Egelman, P. De Camilli, V. M. Unger, *Cell* **132**, 807-17 (2008).
8. M. Gavutis, S. Lata, P. Lamken, P. Muller, J. Piehler, *Biophys J* **88**, 4289-302 (2005).
9. M. Gavutis, S. Lata, J. Piehler, *Nat Protoc* **1**, 2091-103 (2006).
10. M. Gavutis, et al. *Biophys J* **88**, 4289-302 (2005).
11. S. Lata, J. Piehler, *Nat Protoc* **1**, 2104-9 (2006).
12. S. Lata, M. Gavutis, R. Tampe, J. Piehler, *J Am Chem Soc* **128**, 2365-72 (2006).
13. S. Lata, M. Gavutis, J. Piehler, *J Am Chem Soc* **128**, 6-7 (2006).
14. M. D. Stuchell-Brereton, J. J. Skalicky, C. Kieffer, M. A. Karren, S. Ghaffarian, W. I. Sundquist, *Nature* **449**, 740-744 (2007).
15. T. Obita, S. Saksena, S. Ghazi-Tabatabai, D. J. Gill, O. Perisic, S. D. Emr, R. L. Williams, *Nature* **449**, 735-739 (2007).
16. B. J. Peter, H. M. Kent, I. G. Mills, Y. Vallis, P. J. G. Butler, P. R. Evans, H. T. McMahon, *Science* **303**, 495-499 (2004).

17. W. Weissenhorn, *J Mol Biol* **351**, 653-61 (2005).

18. T. H. Millard, G. Bompard, M. Y. Heung, T. R. Dafforn, D. J. Scott, L. M. Machesky, K. Futterer, *EMBO J* **24**, 240-50 (2005).

19. A. Shimada *et al.*, *Cell* **129**, 761-72 (2007).

20. A. Zamborlini, Y. Usami, S. R. Radoshitzky, E. Popova, G. Palu, H. Gottlinger, *Proc Nat Acad Sci U.S.A.* **103**, 19140-19145 (2006).

21. R. D. Fisher, H.-Y. Chung, Q. Zhai, H. Robinson, W. I. Sundquist, C. P. Hill, *Cell* **128**, 841-852 (2007).

22. L. V. Chernomordik, M. M. Kozlov, *Annual Review of Biochemistry* **72**, 175-207 (2003).